

Superconducting switching jump induced missing first Shapiro step in Al-InSb nanosheet Josephson junctions

Xingjun Wu,¹ Haitian Su,^{2,3} Chuanchang Zeng,¹ Ji-Yin Wang,¹ Shili Yan,¹ Dong Pan,^{4,*} Jianhua Zhao,⁴ Po Zhang,^{1,†} and H. Q. Xu^{2,1,‡}

¹*Beijing Academy of Quantum Information Sciences, Beijing 100193, China*

²*Beijing Key Laboratory of Quantum Devices, Key Laboratory for the Physics and Chemistry of Nanodevices, and School of Electronics, Peking University, Beijing 100871, China*

³*Institute of Condensed Matter and Material Physics, School of Physics, Peking University, Beijing 100871, China*

⁴*State Key Laboratory of Superlattices and Microstructures, Institute of Semiconductors, Chinese Academy of Sciences, P.O. Box 912, Beijing 100083, China*

The absence of odd-order Shapiro steps is one of the predicted signatures for topological superconductors. Experimentally, the missing first-order Shapiro step has been reported in several superconducting systems presumably to be topologically non-trivial, as well as in the topologically trivial regime of superconductor-semiconductor Josephson junctions. In this work, we revisit the missing first Shapiro step signature in the topologically trivial regime of Al-InSb nanosheet Josephson junctions under microwave irradiation. The missing first Shapiro step is found to be accompanied by a sharp voltage jump during the superconducting switching and reappears when the jump is softened by increasing temperature or magnetic field. The missing first Shapiro step also reappears with an increased microwave frequency. The sharp switching jump, existing without microwave irradiation, deviates from the relation given by the standard resistively shunted junction (RSJ) model. Missing Shapiro step signatures are qualitatively captured by introducing the sharp voltage jump into the RSJ model. This work reveals a common, yet overlooked, phenomenon that leads to the missing first Shapiro step, providing a new perspective on fractional Josephson experiments.

Topological materials with special energy band structures have received widespread attention in the past few decades [1–9]. Experimental discoveries of new topological states rely on a series of unique signatures, termed “smoking gun” signatures. Examples of smoking gun signatures for topological materials are quantized conductance in transport experiments [10–14] and distinctive energy spectrum patterns in the angle-resolved photoemission spectroscopy [15–17]. Despite witnessing great success, smoking gun signatures do have elusive origins in systems such as the topological superconductor [18–26]. Controversial conclusions may be drawn due to the complexity of real mesoscopic devices compared to a theoretical model, human bias in searching for a target phenomenon, and the lack of proper understanding of a new signature. To determine whether a new topological phase has been achieved and to understand the physics behind experimental signatures, it is essential to explore these signatures in more deterministic systems.

Topological superconductors hosting Majorana zero modes have potential application for realizing the physically protected topological qubit [4, 8, 9, 27–30]. While this kind of qubit has not been invented, the hunting for Majorana zero modes has led to a surging number of works exploring related experimental signatures [31–42]. The simplest and the most famous signatures in transport experiments are the zero-bias conductance peak and the missing Shapiro steps. In this manuscript, we focus on the missing Shapiro step signature.

The missing odd-order Shapiro steps, or the fractional AC Josephson effect, can be understood as follows. In

microwave-illuminated conventional Josephson junctions (JJs), quantized voltage plateaus (Shapiro steps) develop due to coherent transport of charge $2e$ Cooper pairs, where e is the elementary charge [43]. These steps occur at $nhf/2e$, where $n = 1, 2, 3, \dots$, h is the Planck constant, and f is the microwave frequency. In JJs consisting of two topological superconductors, quasiparticles with half the charge of a Cooper pair is transferred, leading to a doubling of Shapiro step voltages [44–52]. The fractional AC Josephson effect can also be understood with the periodicity of a JJ’s current-phase relation (CPR). A topological JJ has a 4π -periodic CPR, rather than the 2π -periodic CPR for conventional JJs. The doubling in periodicity leads to the doubling of Shapiro step voltages, i.e., the disappearance of odd-order steps [53]. Overlapping of Majorana zero modes in a finite system introduces a gap in the energy spectrum and brings a 2π Josephson component. However, the 4π term holds thanks to the topological protection [54]. Besides the fractional AC Josephson effect, topologically trivial mechanisms, including Landau-Zener transition [51, 55] and non-constant resistance [56], are also proposed to cause the missing odd-order Shapiro steps. The Joule heating can cause the disappearance of a continuous series of Shapiro steps starting from the first [57, 58].

Experimentally, the missing first Shapiro step is reported in a variety of materials presumably to be topologically non-trivial, including hybrid junctions combining s-wave superconductors and semiconductor nanowires, topological insulators, or Dirac semimetals [34, 40–42, 59–61]. A stronger evidence with a series of missing

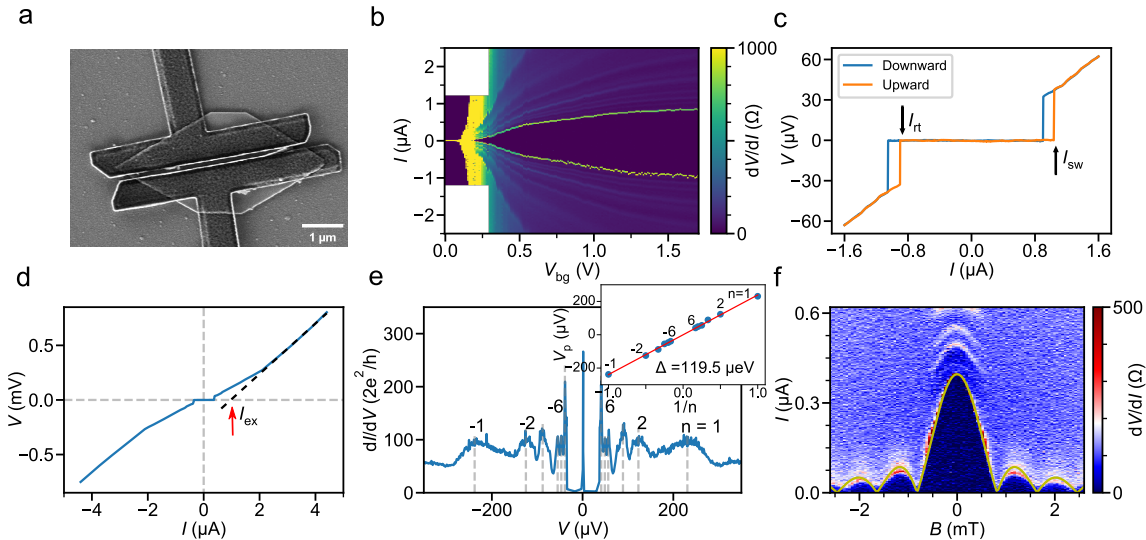


FIG. 1. Device A characterization. (a) Scanning electron microscopy image of device A. The InSb nanosheet (bright gray) is in a hexagonal shape. Two T-shaped superconducting leads (Ti/Al, dark gray) are above the nanosheet. The metallic backgate (Ti/Au) is underneath the nanosheet and extends beyond the displayed range. (b) Differential resistance dV/dI as a function of bias current I and backgate voltage V_{bg} . (c) Hysteresis in $V - I$ curves scanned in the downward (blue) and upward (orange) directions. Retrapping (I_{rt}) and switching (I_{sw}) currents are indicated for the upward scanned curve. $V_{bg} = 2$ V. (d) Voltage-current characteristic at $V_{bg} = 0.5$ V. The dashed fitting line extrapolates to a finite excess current I_{ex} at $V = 0$ (red arrow). (e) Differential conductance dI/dV as a function of voltage bias V . The vertical dashed lines indicate peak positions due to multiple Andreev reflections, which are used for the fitting (red line) in the inset. An induced gap of $119.5 \mu\text{eV}$ is extracted. $V_{bg} = 0.5$ V. (f) Differential resistance dV/dI as a function of I and the magnetic field B . The yellow line is the switching current fitted with the theoretical Fraunhofer curve. $V_{bg} = 0.5$ V.

odd-order Shapiro steps is reported in the Al-HgTe 2D topological insulator system only [38]. Experiments in the topologically trivial regime are performed in the Al-InAs quantum well hybrid system under zero magnetic field, where both missing first [21] and multiple odd-order Shapiro steps [62] are reported.

Even though both theory and experiments have shown that missing odd-order Shapiro steps, especially the missing first Shapiro step, have non-topological origins, the underlying mechanism and how common this mechanism is in experiments, as we will show in this work, remain to be understood.

LIST OF KEY RESULTS

We study Shapiro steps in Al-InSb nanosheet-based JJs. Instead of growing both materials in the same molecular beam epitaxy (MBE) machine, the Al layer is grown ex-situ using conventional nanofabrication methods. The magnetic field is either set to be zero or the order of millitesla, much smaller than the field required for a topological transition [63]. Therefore, we study the system in the topologically trivial regime. The first

Shapiro step is missing at low frequencies and reappears at higher frequencies. The voltage-current characteristic, taken without microwave irradiation, manifests a sharp voltage jump near the superconducting switching. The sharp jump deviates from the relation established by the standard resistively shunted junction (RSJ) model. The absence of the first Shapiro step persists in the intermediate temperature regime where the hysteresis caused by Joule heating is suppressed, while the sharp switching remains. At a higher temperature or in magnetic fields, we observe further softening of the switching and the reappearance of the missing first Shapiro step. The missing Shapiro step behaviors are qualitatively captured by a conceptual model with switching jumps. In addition to the missing first Shapiro step, we observe a residual supercurrent at the first node of the zeroth Shapiro lobes and a suppression of the third Shapiro step.

METHODS

High-quality free-standing InSb nanosheets are grown by MBE. These nanosheets typically have dimensions on the order of micrometers in length and width, 10

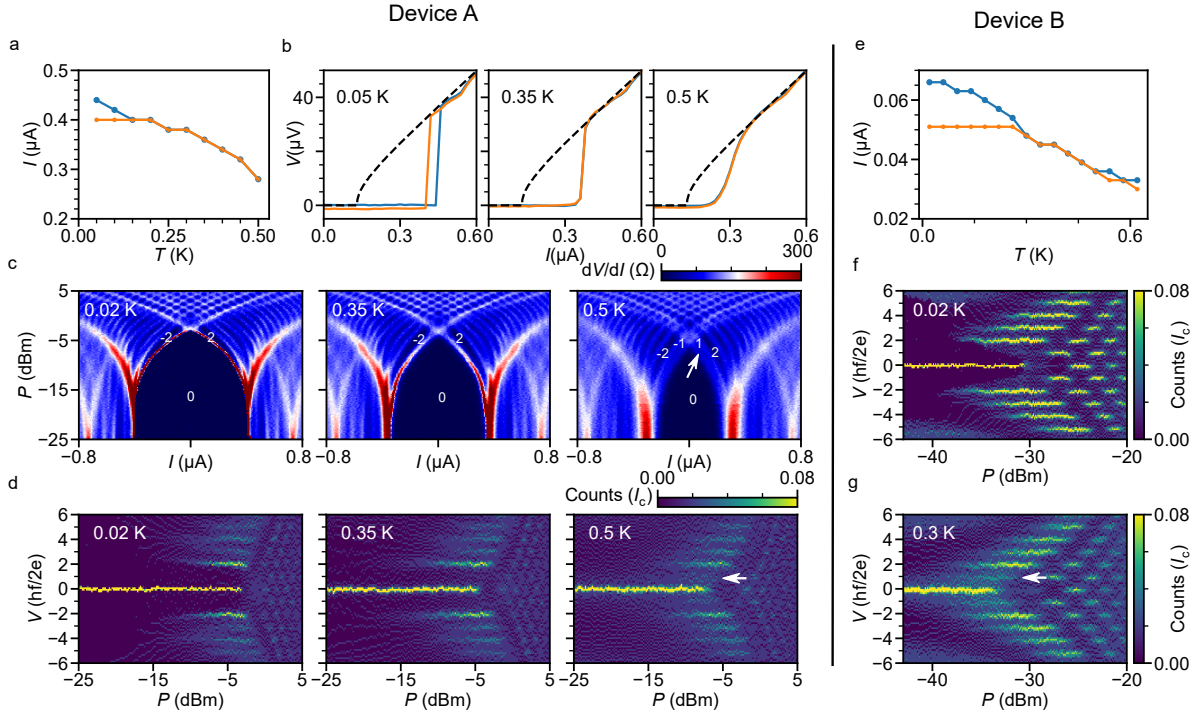


FIG. 2. Temperature dependence of the missing first Shapiro step and the sharp switching jump. (a)-(d) are from device A. (e)-(g) are from device B. (a) The switching current (blue) and retrapping current (orange) as a function of the temperature T . (b) Voltage-current characteristics at 0.05, 0.35, and 0.5 K without microwave irradiation. The blue (orange) curve is scanned in the positive (negative) direction. Dashed lines are fitting curves using the relation from the RSJ model. The sharp superconducting switching jump softens as the temperature increases. (c) Differential resistance dV/dI as a function of microwave power P and DC bias current I at 0.02, 0.35, and 0.5 K. (d) Corresponding voltage histograms of (c). (e) Switching current (blue) and retrapping current (orange) from device B. (f) and (g) Histogram maps of device B at 0.02 and 0.3 K, respectively. White arrows in (c), (d), and (g) indicate reappearance of the missing first Shapiro step at higher temperatures. The microwave frequency is 2.5 GHz for both devices. The bin size for all histogram maps is 0.14.

to 100 nm in thickness. The low-temperature mobility is above 10^4 cm²/Vs. Details about the material and transport properties can be found in Refs. [64, 65]. Two devices are studied in the main text, termed devices A and B. Nanosheets are transferred to the substrate by a micromanipulator. Local Ti/Au backgates are pre-patterned before depositing nanosheets. Native oxide on the surface of the nanosheet is removed by sulfur passivation [65, 66]. The superconducting leads are patterned by e-beam lithography followed by evaporating 5/110 nm Ti/Al. The junction width and length are 4.2 (1.9) μ m and 110 (120) nm in device A (B).

Measurements are performed in a dilution refrigerator with a base temperature of about 15 mK. The microwave is coupled to junctions via an antenna. Attenuators of 29 dB in total are installed in the microwave line [67]. The power value marked in the manuscript is the power on the microwave source. A numeric offset of about 3.5 mT is applied to the magnetic field. The offset

may arise due to fluxes trapped in the magnet. The voltage is shifted by values of the order of μ V to compensate for DC offsets in amplifiers and thermal voltages in lines.

FIGURE 1 DESCRIPTION

The characterization of device A is presented in Fig. 1. Two T-shaped Ti/Al leads and the InSb in between form a JJ (Fig. 1a). Superconductivity of the junction can be tuned by the metallic backgate underneath the nanosheet. The turn-on backgate voltage is about 0.2 V (Fig. 1b). The switching/retrapping currents reach $-1/0.8$ μ A as V_{bg} increases to 1.7 V. Dark fringes alongside the central zero-resistance lobe are due to multiple Andreev reflections (MARs). The difference between switching and retrapping currents indicates a hysteresis regarding the current, which is shown more clearly in Fig. 1c.

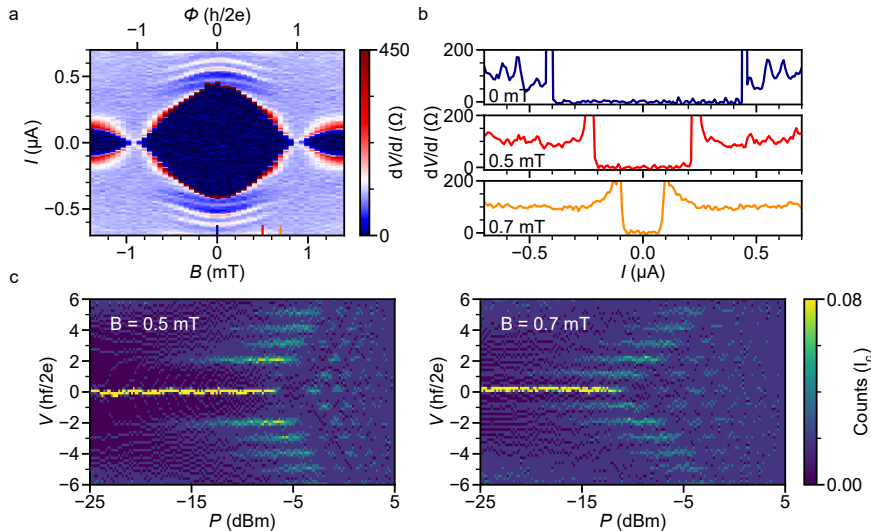


FIG. 3. Magnetic field dependence of the missing first Shapiro step in device A. (a) Differential resistance dV/dI as a function of current I and magnetic field B , without microwave irradiation. Three short vertical lines near the bottom axis indicate magnetic fields where curves in (b) are extracted. (b) Linecuts from (a) taken at fixed magnetic fields. The magnetic fields are indicated in each subpanel. The dV/dI peaks near superconducting switchings are broadened by the magnetic field. (c) Voltage histograms taken at a microwave frequency of 2.5 GHz. The magnetic field is indicated in white text. The bin size is 0.17. The zero field histogram can be found in Fig. 2d.

The typical excess current I_{ex} and normal-state resistance R_n are extracted from the fit to the linear regime in Fig. 1d, which gives $I_{ex} = 0.97 \mu\text{A}$, $R_n = 230 \Omega$, and an $I_{ex}R_n$ product of $223 \mu\text{V}$. We estimate an induced superconducting gap Δ of $119.5 \mu\text{eV}$ by fitting positions of MARs to $V = 2\Delta/ne$, $n = \pm 1, \pm 2, \dots, \pm 6$ (Fig. 1e). The induced gap is roughly half of the value reported in devices with epitaxial Al layer [68]. The small induced gap is expected because, in this work, the Al layer is grown using conventional nanofabrication methods. Despite a smaller gap, the device manifests high-quality coherent transport properties, demonstrated by MARs up to an order of six. This is likely because the Andreev reflection does not take place at the physical superconductor-semiconductor interface and the high mobility in the junction's normal region [69]. We extract a high transparency T_r of 0.9 using the Octavio-Tinkham-Blonder-Klapwijk (OTBK) model [70], given that $eI_{ex}R_n/\Delta = 1.86$.

In magnetic fields, the switching current oscillates following the Fraunhofer diffraction pattern (Fig. 1f), indicating a uniform current distribution in the device. The period 0.8 mT gives an effective junction length of about 600 nm, which is larger than the designed junction length (110 nm). The larger effective length is likely due to the London penetration [65, 71].

FIGURE 2 DESCRIPTION

The key observation on the missing first Shapiro step is presented in Fig. 2. The extracted switching and retrapping current curves merge at 0.15 K (Fig. 2a), indicating that the hysteresis originates from the Joule heating effect [72]. Besides the hysteresis, we observe sharp superconducting switching jumps in the voltage-current characteristics (Fig. 2b). At 0.05 K, the curve manifests both sharp switchings and hysteresis. For instance, in the upward scan (blue), the voltage abruptly jumps from 0 V at $0.44 \mu\text{A}$ to $37 \mu\text{V}$ at $0.46 \mu\text{A}$. This sharp jump, despite common in experiments, is inconsistent with the relation derived from the standard RSJ model, $V \propto \sqrt{I^2 - I_c^2}$ (dashed lines), where I_c is the critical current [73, 74]. The sharp jump persists at 0.35 K while the hysteresis is not visible at this temperature, indicating that the jump is independent of the hysteresis. At 0.5 K the switching is much softer with a smaller slope near the switching current. The softening of the switching is also confirmed by the broadening of dV/dI peaks at -25 dBm in Fig. 2c.

Next, we turn on the microwave irradiation and study Shapiro steps. A Shapiro step is a minimum in the dV/dI maps (Fig. 2c) or a maximum in the histograms (Fig. 2d). We are interested in Shapiro steps at power values smaller than the first node of the zeroth Shapiro step lobe [21, 38]. The first Shapiro step is missing at 0.02

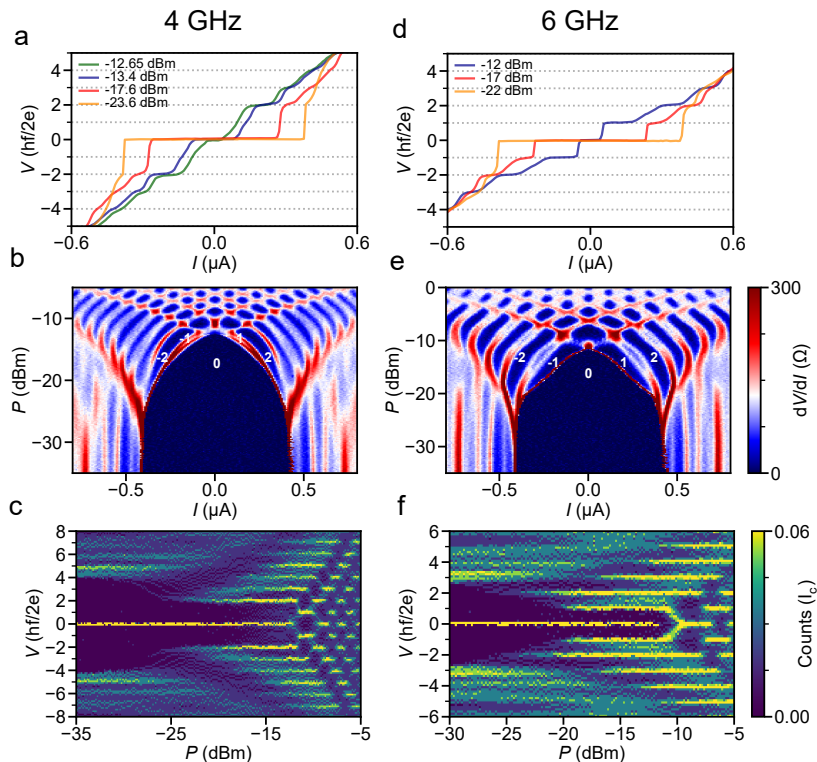


FIG. 4. Frequency dependence of the missing first Shapiro step in device A. (a) Voltage-current characteristics at a variety of microwave powers at 4 GHz. The voltage is normalized by $hf/2e$, thus the value corresponds to the Shapiro index. (b) Differential resistance dV/dI as a function of microwave power P and current I at a microwave frequency of 4 GHz. Shapiro step indexes are indicated in white text. (c) Voltage histograms that correspond to (b). The bin size is 0.14. (d)-(f) Similar to (a)-(c) but measured at a frequency of 6 GHz. The 2.5 GHz response can be found in Fig. 2.

and 0.35 K. Furthermore, at 0.02 K the sharp switching leaves a dark regime between $V = 0$ and 2 (Fig. 2d), meaning that there are no data points collected in this voltage range due to the sharp switching. In contrast, the region between $V = 2$ and 3 is relatively brighter. At 0.35 K, the area between $V = 0$ and 2 becomes brighter due to a slight softening of the switching. At 0.5 K, although thermal fluctuations obscure the Shapiro map, the reappearance of the first Shapiro step is still visible. This can be confirmed by looking at either the splitting of dV/dI peaks in Fig. 2c (white arrow) or the voltage histogram in Fig. 2d (white arrow).

Similar behaviors are observed in device B (Figs. 2e-2g). Unlike in device A, the missing first Shapiro step in device B reappears as soon as the hysteresis disappears at 0.3 K. We do not observe an intermediate regime where the hysteresis disappears while the first Shapiro step is still missing.

FIGURE 3 DESCRIPTION

The magnetic-field dependence of the missing Shapiro step in device A is depicted in Fig. 3. We first study the response without microwave irradiation. Fig. 3a shows a zoomed-in view of Fig. 1f near zero field. Vertical cuts along $B = 0, 0.5,$ and 0.7 mT are extracted and depicted in Fig. 3b. Similar to the temperature, the magnetic field not only reduces the critical current but also widens the dV/dI peaks at the superconducting switching. The broadening of the dV/dI peaks above 0.5 mT can be observed in both Figs. 3a and 3b.

Under microwave irradiation, the first Shapiro step reappears at 0.7 mT (Fig. 3c). In the intermediate regime where the field is 0.5 mT, the onset of the first missing Shapiro step occurs near -5.6 dBm. In the histogram, there are still dark regions with small bin counts near $V = \pm 1$ and $P < -7$ dBm, indicating that the switching is still sharp. At 0.7 mT, the same area is brighter, and the stripe of the first Shapiro step is observed.

Another interesting effect is the suppression of higher odd-order Shapiro steps, here the third Shapiro step. The

onset power of the third step is larger than that of the two adjacent steps at 0 and 0.5 mT. As a comparison, the onset power increases monotonically with the Shapiro index at 0.7 mT. Similar suppression is reported in the trivial regime of the Al-InAs quantum well system [21, 62]. The non-topological origin of the suppression could be either Landau-Zener transition or non-linear resistance due to MARs [56]. The latter explanation is favored in this work because the suppression disappears once the MARs are smoothed out by increasing the magnetic field to 0.7 mT (Fig. 3a and 3c).

FIGURE 4 DESCRIPTION

We study the frequency dependence of the missing Shapiro steps in Fig. 4. At an increased microwave frequency of 4 GHz (Figs. 4a-4c), the dV/dI peak between dips corresponding to steps 0 and 2 splits. The splitting indicates the onset of the first Shapiro step (labeled “1”) that is not visible at 2.5 GHz. The first Shapiro step is still indiscernible in the corresponding histogram (Fig. 4c) because the step is not well quantized. The bin counts within the region where $P < -15$ dBm and $0 < V < 2$ are close to zero, resulting in a dark appearance for this area. Below -25 dBm, the dark area extends to $V = 4$, “eliminating” Shapiro steps 1, 2, and 3. This is another piece of evidence that indicates missing Shapiro steps are caused by the sharp switching jump.

At a higher frequency of 6 GHz (Figs. 4d-4f), the first step is clearly established. In addition to the reappearance of the first step, we observe half-integer steps at 6 GHz. The most apparent half step is the $3/2$ step, which is a dip in dV/dI between dark blue areas labeled “1” and “2” or the bright stripe at $V = 1.5$ in the histogram. Higher-order half-integer steps are also observed. However, the first half-integer step, the “ $1/2$ ” step, is missing. Similar results are reported in the quantum well system [62]. We attribute it also to the sharp switching in the V-I curve, evidenced by the near zero bin counts at $V = \pm 1/2$.

A residual supercurrent at the node of the zeroth Shapiro step lobe is observed in Fig. 4b. A zoomed-in view of this figure and residual supercurrent in device B can be found in Fig. S3. The residual supercurrent is also a signature for topological superconductors [41, 75]. However, higher-order Josephson harmonics in the CPR of a JJ can also mimic this feature (Fig. S8).

DISCUSSION

Previous works on the missing Shapiro steps were carried out in systems presumably to be topologically non-trivial or in the non-topological regime of the Al-InAs quantum well system [21, 62]. The latter has supercon-

ducting layers grown using dedicated methods combining MBE, in-situ growth or hydrogen plasma cleaning, and cryogenic temperature growth techniques, which are not used in many topological experiments [69, 76, 77]. These techniques guarantee a sharp superconductor-semiconductor interface and the uniformity of the superconducting layer [78, 79]. Devices made with conventional nanofabrication methods in this work have an induced gap about half the typical size of epitaxial Al devices [36, 76, 77, 80]. Since many works regarding the missing Shapiro steps do not employ the epitaxial method, devices in this work serve as a better comparison platform for topological superconductor studies. The observation of the missing first Shapiro and other signatures in this work reveals that these signatures are unexpectedly common in experiments.

Several pieces of evidence indicate that the missing first Shapiro step is caused by the sharp superconducting switching. First, the bin counts are close to zero at $V = \pm 1$ when the first step is missing. The small bin count is an indicator of a violent voltage change. In addition, the first step reappears when the jump is softened. Second, the disappearance of the $1/2$ Shapiro step, and the elimination of all Shapiro steps below $V = 4$ by the extension of the dark region in histograms. These missing steps can be understood in the same way as the disappearance of the first Shapiro step. In contrast, Majorana physics or Landau-Zener transition fails to include these missing steps. Third, the frequency dependence favors the sharp switching jump scenario over the Landau-Zener transition scenario. The former mechanism is enhanced with a decreased frequency because the lower the frequency, the smaller and more fragile the Shapiro step voltages compared to the fixed jump voltage. The latter mechanism, however, is weakened with a decreased frequency. The missing first Shapiro step, the frequency dependence, and the extension of the dark region at lower powers are qualitatively captured by a conceptual model where the voltage jump is introduced by adding a shunted capacitance (Fig. S7).

The origins of the sharp switching remain to be understood. Any premature transition into the normal state can cause a sharp voltage jump. A well-known effect is the Joule heating. It is demonstrated that the heating effect can lead to the missing of a continuous series of Shapiro steps starting from the first one. However, the heating effect or the capacitance effect is usually accompanied by a hysteresis regarding the current, while in our devices the sharp switching and the missing first Shapiro step can occur without obvious hysteresis.

Another possible origin of the sharp switching is the premature transition to the normal state due to the suppression of switching currents caused by finite voltage processes, e.g., the MARs. A similar premature transition is reported to cause the enhancement of the critical current in the presence of a magnetic field, another

“smoking gun” signature of the topological superconductor favoring a triplet pairing [26]. In Fig. 3a, fringes of MARs intersect with the superconducting switching boundary, indicating the competition between the finite voltage state and the superconducting state. Fluctuations may drive the system into the finite-voltage MAR states, leading to a sharp switching.

In conclusion, the observation of the missing first Shapiro step, together with other signatures, in the topologically trivial regime of Al-InSb nanosheet JJs reveals the unexpected ubiquity of these signatures. The missing first Shapiro step is attributed to sharp superconducting switchings in voltage-current characteristics taken without microwave irradiation, a common but not well-recognized phenomenon in real devices. Even though the experiment is conducted in a preset topologically trivial regime, the analysis employed in this study does not depend on any prior knowledge regarding the system’s topological properties. Therefore, it can be employed in demonstrating the presence of topological states in other materials. Future Majorana works may focus on improving the quality and tunability of devices. The smoking gun signature paradigm should still work by deeper analysis of larger volumes of data, including data from comparison experiments made with topologically trivial systems [26].

DATA AVAILABILITY

Data, processing code, and simulation code are available at Ref. [81]

ACKNOWLEDGEMENTS

This work is supported by the NSFC (Grant Nos. 92165208, 12004039, 11874071, 92365103, 12374480, 12374459, 61974138 and 92065106). D.P. acknowledges the support from Youth Innovation Promotion Association, Chinese Academy of Sciences (Nos. 2017156 and Y2021043).

AUTHOR CONTRIBUTIONS

H.Q.X. supervised the project. X.W., H.S., and S.Y. fabricated devices. X.W., H.S., and J.-Y.W. performed measurements. C.Z. and P.Z. did the simulation. D.P. and J.Z. developed the nanosheet material. X.W., P.Z., and H.Q.X. analyzed the data and wrote the manuscript with inputs from all authors.

* pandong@semi.ac.cn

† zhangpo@baqis.ac.cn

‡ hqxu@pku.edu.cn

- [1] D. J. Thouless, M. Kohmoto, M. P. Nightingale, and M. den Nijs, Phys. Rev. Lett. **49**, 405 (1982).
- [2] Q. Niu, D. J. Thouless, and Y.-S. Wu, Phys. Rev. B **31**, 3372 (1985).
- [3] B. I. Halperin, P. A. Lee, and N. Read, Phys. Rev. B **47**, 7312 (1993).
- [4] A. Y. Kitaev, Physics-Uspekhi **44**, 131 (2001).
- [5] C. L. Kane and E. J. Mele, Phys. Rev. Lett. **95**, 146802 (2005).
- [6] B. A. Bernevig, T. L. Hughes, and S.-C. Zhang, science **314**, 1757 (2006).
- [7] L. Fu, C. L. Kane, and E. J. Mele, Phys. Rev. Lett. **98**, 106803 (2007).
- [8] R. M. Lutchyn, J. D. Sau, and S. Das Sarma, Phys. Rev. Lett. **105**, 077001 (2010).
- [9] Y. Oreg, G. Refael, and F. von Oppen, Phys. Rev. Lett. **105**, 177002 (2010).
- [10] K. v. Klitzing, G. Dorda, and M. Pepper, Phys. Rev. Lett. **45**, 494 (1980).
- [11] D. C. Tsui, H. L. Stormer, and A. C. Gossard, Phys. Rev. Lett. **48**, 1559 (1982).
- [12] M. König, S. Wiedmann, C. Brüne, A. Roth, H. Buhmann, L. W. Molenkamp, X.-L. Qi, and S.-C. Zhang, Science **318**, 766 (2007).
- [13] I. Knez, R.-R. Du, and G. Sullivan, Phys. Rev. Lett. **107**, 136603 (2011).
- [14] C.-Z. Chang, J. Zhang, X. Feng, J. Shen, Z. Zhang, M. Guo, K. Li, Y. Ou, P. Wei, L.-L. Wang, *et al.*, Science **340**, 167 (2013).
- [15] D. Hsieh, D. Qian, L. Wray, Y. Xia, Y. S. Hor, R. J. Cava, and M. Z. Hasan, Nature **452**, 970 (2008).
- [16] S.-Y. Xu, I. Belopolski, N. Alidoust, M. Neupane, G. Bian, C. Zhang, R. Sankar, G. Chang, Z. Yuan, C.-C. Lee, S.-M. Huang, H. Zheng, J. Ma, D. S. Sanchez, B. Wang, A. Bansil, F. Chou, P. P. Shibayev, H. Lin, S. Jia, and M. Z. Hasan, Science **349**, 613 (2015).
- [17] B. Q. Lv, H. M. Weng, B. B. Fu, X. P. Wang, H. Miao, J. Ma, P. Richard, X. C. Huang, L. X. Zhao, G. F. Chen, Z. Fang, X. Dai, T. Qian, and H. Ding, Phys. Rev. X **5**, 031013 (2015).
- [18] J. Chen, B. D. Woods, P. Yu, M. Hocevar, D. Car, S. R. Plissard, E. P. A. M. Bakkers, T. D. Stanescu, and S. M. Frolov, Phys. Rev. Lett. **123**, 107703 (2019).
- [19] M. Kayyalha, D. Xiao, R. Zhang, J. Shin, J. Jiang, F. Wang, Y.-F. Zhao, R. Xiao, L. Zhang, K. M. Fijalkowski, P. Mandal, M. Winnerlein, C. Gould, Q. Li, L. W. Molenkamp, M. H. W. Chan, N. Samarth, and C.-Z. Chang, Science **367**, 64 (2020).
- [20] P. Yu, J. Chen, M. Gomanko, G. Badawy, E. P. A. M. Bakkers, K. Zuo, V. Mourik, and S. M. Frolov, Nature Physics **17**, 482 (2021).
- [21] M. C. Dartiaillh, J. J. Cuzzo, B. H. Elfeky, W. Mayer, J. Yuan, K. S. Wickramasinghe, E. Rossi, and J. Shabani, Nature Communications **12**, 78 (2021).
- [22] M. Valentini, F. Peñaranda, A. Hofmann, M. Brauns, R. Hauschild, P. Krogstrup, P. San-Jose, E. Prada, R. Aguado, and G. Katsaros, Science **373**, 82 (2021).

- [23] M. Valentini, M. Borovkov, E. Prada, S. Martí-Sánchez, M. Botifoll, A. Hofmann, J. Arbiol, R. Aguado, P. San-Jose, and G. Katsaros, *Nature* **612**, 442 (2022).
- [24] Y. Sato, K. Ueda, Y. Takeshige, H. Kamata, K. Li, L. Samuelson, H. Q. Xu, S. Matsuo, and S. Tarucha, *Phys. Rev. Lett.* **128**, 207001 (2022).
- [25] J.-Y. Wang, N. van Loo, G. P. Mazur, V. Levajac, F. K. Malinowski, M. Lemang, F. Borsoi, G. Badawy, S. Gazibegovic, E. P. A. M. Bakkers, M. Quintero-Pérez, S. Heedt, and L. P. Kouwenhoven, *Phys. Rev. B* **106**, 075306 (2022).
- [26] S. Frolov, P. Zhang, B. Zhang, Y. Jiang, S. Byard, S. Mudi, J. Chen, A.-H. Chen, M. Hocevar, M. Gupta, *et al.*, arXiv preprint arXiv:2309.09368 (2023).
- [27] N. Read and D. Green, *Phys. Rev. B* **61**, 10267 (2000).
- [28] A. Y. Kitaev, *Annals of physics* **303**, 2 (2003).
- [29] C. Nayak, S. H. Simon, A. Stern, M. Freedman, and S. Das Sarma, *Rev. Mod. Phys.* **80**, 1083 (2008).
- [30] L. Fu and C. L. Kane, *Phys. Rev. Lett.* **100**, 096407 (2008).
- [31] V. Mourik, K. Zuo, S. M. Frolov, S. R. Plissard, E. P. A. M. Bakkers, and L. P. Kouwenhoven, *Science* **336**, 1003 (2012).
- [32] M. Deng, C. Yu, G. Huang, M. Larsson, P. Caroff, and H. Xu, *Nano letters* **12**, 6414 (2012).
- [33] A. Das, Y. Ronen, Y. Most, Y. Oreg, M. Heiblum, and H. Shtrikman, *Nature Physics* **8**, 887 (2012).
- [34] L. P. Rokhinson, X. Liu, and J. K. Furdyna, *NATURE PHYSICS* **8**, 795 (2012).
- [35] S. Nadj-Perge, I. K. Drozdov, J. Li, H. Chen, S. Jeon, J. Seo, A. H. MacDonald, B. A. Bernevig, and A. Yazdani, *Science* **346**, 602 (2014).
- [36] M. T. Deng, S. Vaitiekėnas, E. B. Hansen, J. Danon, M. Leijnse, K. Flensberg, J. Nygård, P. Krogstrup, and C. M. Marcus, *Science* **354**, 1557 (2016).
- [37] H.-H. Sun, K.-W. Zhang, L.-H. Hu, C. Li, G.-Y. Wang, H.-Y. Ma, Z.-A. Xu, C.-L. Gao, D.-D. Guan, Y.-Y. Li, *et al.*, *Phys. Rev. Lett.* **116**, 257003 (2016).
- [38] E. Bocquillon, R. S. Deacon, J. Wiedenmann, P. Leubner, T. M. Klapwijk, C. Bruene, K. Ishibashi, H. Buhmann, and L. W. Molenkamp, *NATURE NANOTECHNOLOGY* **12**, 137 (2017).
- [39] D. Wang, L. Kong, P. Fan, H. Chen, S. Zhu, W. Liu, L. Cao, Y. Sun, S. Du, J. Schneeloch, *et al.*, *Science* **362**, 333 (2018).
- [40] C. Li, J. C. de Boer, B. de Ronde, S. V. Ramankutty, E. van Heumen, Y. Huang, A. de Visser, A. A. Golubov, M. S. Golden, and A. Brinkman, *Nature Materials* **17**, 875 (2018).
- [41] A.-Q. Wang, C.-Z. Li, C. Li, Z.-M. Liao, A. Brinkman, and D.-P. Yu, *Phys. Rev. Lett.* **121**, 237701 (2018).
- [42] I. T. Rosen, C. J. Trimble, M. P. Andersen, E. Mikheev, Y. Li, Y. Liu, L. Tai, P. Zhang, K. L. Wang, Y. Cui, *et al.*, arXiv preprint arXiv:2110.01039 (2021).
- [43] B. D. Josephson, *Physics letters* **1**, 251 (1962).
- [44] H. Kwon, K. Sengupta, and V. Yakovenko, *EUROPEAN PHYSICAL JOURNAL B* **37**, 349 (2004).
- [45] L. Fu and C. L. Kane, *Phys. Rev. B* **79**, 161408 (2009).
- [46] L. Jiang, D. Pekker, J. Alicea, G. Refael, Y. Oreg, and F. von Oppen, *Phys. Rev. Lett.* **107**, 236401 (2011).
- [47] D. M. Badiane, M. Houzet, and J. S. Meyer, *Phys. Rev. Lett.* **107**, 177002 (2011).
- [48] P. San-Jose, E. Prada, and R. Aguado, *Phys. Rev. Lett.* **108**, 257001 (2012).
- [49] F. Domínguez, F. Hassler, and G. Platero, *Phys. Rev. B* **86**, 140503 (2012).
- [50] M. Houzet, J. S. Meyer, D. M. Badiane, and L. I. Glazman, *Phys. Rev. Lett.* **111**, 046401 (2013).
- [51] J. D. Sau and F. Setiawan, *Phys. Rev. B* **95**, 060501 (2017).
- [52] Y.-H. Li, J. Song, J. Liu, H. Jiang, Q.-F. Sun, and X. C. Xie, *Phys. Rev. B* **97**, 045423 (2018).
- [53] J. Park, Y.-B. Choi, G.-H. Lee, and H.-J. Lee, *Phys. Rev. B* **103**, 235428 (2021).
- [54] D. I. Pikulin and Y. V. Nazarov, *Phys. Rev. B* **86**, 140504 (2012).
- [55] J. D. Sau, E. Berg, and B. I. Halperin, arXiv preprint arXiv:1206.4596 (2012).
- [56] S. R. Mudi and S. M. Frolov, Model for missing shapiro steps due to bias-dependent resistance (2022), arXiv:2106.00495 [cond-mat.mes-hall].
- [57] A. De Cecco, K. Le Calvez, B. Sacépé, C. B. Winkelmann, and H. Courtois, *Phys. Rev. B* **93**, 180505 (2016).
- [58] C. D. Shelly, P. See, I. Rungger, and J. M. Williams, *Phys. Rev. Appl.* **13**, 024070 (2020).
- [59] J. Wiedenmann, E. Bocquillon, R. S. Deacon, S. Hartinger, O. Herrmann, T. M. Klapwijk, L. Maier, C. Ames, C. Bruene, C. Gould, A. Oiwa, K. Ishibashi, S. Tarucha, H. Buhmann, and L. W. Molenkamp, *NATURE COMMUNICATIONS* **7**, 10.1038/ncomms10303 (2016).
- [60] W. Yu, W. Pan, D. L. Medlin, M. A. Rodriguez, S. R. Lee, Z.-q. Bao, and F. Zhang, *Phys. Rev. Lett.* **120**, 177704 (2018).
- [61] M. Bai, X.-K. Wei, J. Feng, M. Luysberg, A. Bliesener, G. Lippertz, A. Uday, A. A. Taskin, J. Mayer, and Y. Ando, *Communications Materials* **3**, 20 (2022).
- [62] P. Zhang, S. Mudi, M. Pendharkar, J. S. Lee, C. P. Dempsey, A. P. McFadden, S. D. Harrington, J. T. Dong, H. Wu, A. H. Chen, M. Hocevar, C. J. Palmstrøm, and S. M. Frolov, Missing odd-order shapiro steps do not uniquely indicate fractional josephson effect (2022), arXiv:2211.08710 [cond-mat.mes-hall].
- [63] M. C. Dartiaillh, W. Mayer, J. Yuan, K. S. Wickramasinghe, A. Matos-Abiague, I. Žutić, and J. Shabani, *Phys. Rev. Lett.* **126**, 036802 (2021).
- [64] D. Pan, D. X. Fan, N. Kang, J. H. Zhi, X. Z. Yu, H. Q. Xu, and J. H. Zhao, *NANO LETTERS* **16**, 834 (2016).
- [65] N. Kang, D. Fan, J. Zhi, D. Pan, S. Li, C. Wang, J. Guo, J. Zhao, and H. Xu, *NANO LETTERS* **19**, 561 (2019).
- [66] D. B. Suyatin, C. Thelander, M. T. Björk, I. Maximov, and L. Samuelson, *Nanotechnology* **18**, 105307 (2007).
- [67] S. Yan, H. Su, D. Pan, W. Li, Z. Lyu, M. Chen, X. Wu, L. Lu, J. Zhao, J.-Y. Wang, and H. Xu, *Nano Letters* **23**, 6497 (2023).
- [68] P. Zhang, H. Wu, J. Chen, S. A. Khan, P. Krogstrup, D. Pekker, and S. M. Frolov, *Phys. Rev. Lett.* **128**, 046801 (2022).
- [69] J. Shabani, M. Kjaergaard, H. J. Suominen, Y. Kim, F. Nichele, K. Pakrouski, T. Stankevic, R. M. Lutchyn, P. Krogstrup, R. Feidenhans'l, S. Kraemer, C. Nayak, M. Troyer, C. M. Marcus, and C. J. Palmstrøm, *Phys. Rev. B* **93**, 155402 (2016).
- [70] M. Octavio, M. Tinkham, G. E. Blonder, and T. M. Klapwijk, *Phys. Rev. B* **27**, 6739 (1983).
- [71] P. Zhang, A. Zarassi, L. Jarjat, V. V. de Sande, M. Pendharkar, J. S. Lee, C. P. Dempsey, A. P. McFadden, S. D. Harrington, J. T. Dong, H. Wu, A. H. Chen, M. Hocevar,

- C. J. Palmstrøm, and S. M. Frolov, *SciPost Phys.* **16**, 030 (2024).
- [72] H. Courtois, M. Meschke, J. T. Peltonen, and J. P. Pekola, *Phys. Rev. Lett.* **101**, 067002 (2008).
- [73] D. McCumber, *Journal of Applied Physics* **39**, 3113 (1968).
- [74] W. Stewart, *Applied physics letters* **12**, 277 (1968).
- [75] K. Le Calvez, L. Veyrat, F. Gay, P. Plaindoux, C. B. Winkelmann, H. Courtois, and B. Sacépé, *Communications Physics* **2**, 4 (2019).
- [76] J. S. Lee, B. Shojaei, M. Pendharkar, A. P. McFadden, Y. Kim, H. J. Suominen, M. Kjaergaard, F. Nichele, H. Zhang, C. M. Marcus, and C. J. Palmstrøm, *Nano Letters* **19**, 3083 (2019).
- [77] P. Zhang, A. Zarassi, M. Pendharkar, J. Lee, L. Jarjat, V. Van de Sande, B. Zhang, S. Mudi, H. Wu, S. Tan, *et al.*, arXiv preprint arXiv:2211.04130 (2022).
- [78] P. Krogstrup, N. L. B. Ziino, W. Chang, S. M. Albrecht, M. H. Madsen, E. Johnson, J. Nygård, C. M. Marcus, and T. S. Jespersen, *Nature Materials* **14**, 400 (2015).
- [79] D. Pan, H. Song, S. Zhang, L. Liu, L. Wen, D. Liao, R. Zhuo, Z. Wang, Z. Zhang, S. Yang, J. Ying, W. Miao, R. Shang, H. Zhang, and J. Zhao, *Chinese Physics Letters* **39**, 058101 (2022).
- [80] F. Nichele, A. C. C. Drachmann, A. M. Whiticar, E. C. T. O'Farrell, H. J. Suominen, A. Fornieri, T. Wang, G. C. Gardner, C. Thomas, A. T. Hatke, P. Krogstrup, M. J. Manfra, K. Flensberg, and C. M. Marcus, *Phys. Rev. Lett.* **119**, 136803 (2017).
- [81] DOI: 10.5281/zenodo.10803799.

Supplementary Materials: Superconducting switching jump induced missing first Shapiro step in Al-InSb nanosheet Josephson junctions

I. DEVICE AND MEASUREMENT INFORMATION

TABLE S1. Device and cooldown reference

Name	Chip	Device	Nanosheet/wire batch	Cooldown
Device A	InSb-Chip-41	JJ-right-s2	InSb-n1362	Triton XL 2023-09-15 to 2023-10-30
Device B	InSb-Chip-41	JJ-right-s5	InSb-n1362	Triton XL 2023-09-15 to 2023-10-30
Device S1	20230111 Al-InAs-Chip-16	JJ-right-5	InAs-epi-Al-2852	Triton XL 2023-02-25 to 2023-03-16

II. ADDITIONAL INFORMATION ON DEVICE B

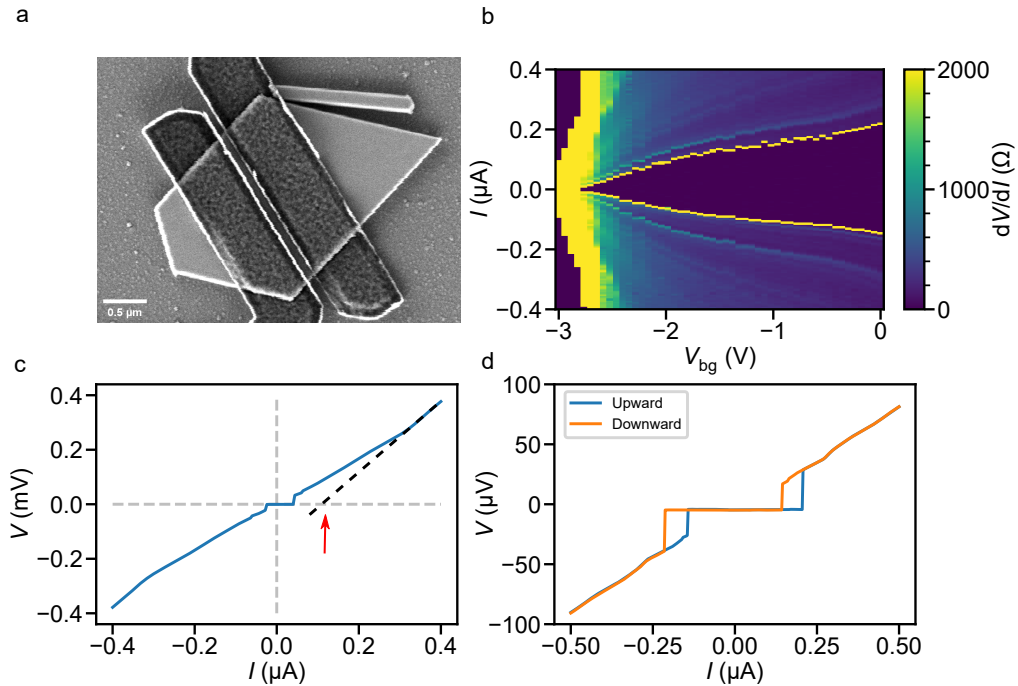


FIG. S1. Characterization of Device B. (a) SEM image. (b) Differential resistance dV/dI as a function of bias current I and back-gate voltage V_{bg} . We note that the supercurrent vanishes at $V_{bg} = 0.2$ V in the initial measurement. Due to the presence of a charge-trapping layer at interfaces, the value drifts to about -2.8 V after applying a large negative gate voltage. The data is repeatable as long as no larger negative gate voltage is applied. (c) Voltage-current characteristic in the junction at $V_{bg} = -2.46$ V. By linearly fitting the $V - I$ characteristic at a high bias range, we extract $I_{ex} = 109$ nA and $R_n = 1.3$ k Ω . Thus, $eI_{ex}R_n/\Delta$ is 0.93, where the induced superconducting gap Δ is determined from the positions of MARs. According to the OTBK model, we obtain the interface transmission ~ 0.7 . (d) Hysteretic behavior in $V - I$ curve at $V_{bg} = 0$ V. Blue and orange curves indicate two opposite directions in sweeping bias current.

III. ADDITIONAL DATA ABOUT THE SUPPRESSION OF HIGHER ODD-ORDER SHAPIRO STEPS ON DEVICE A

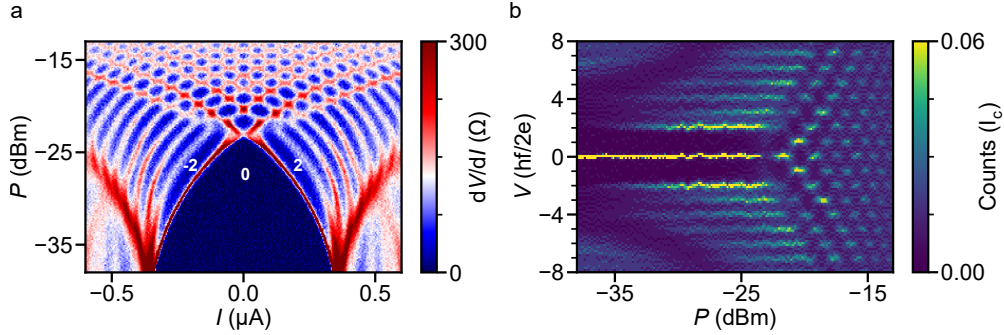


FIG. S2. Suppression of the third Shapiro step on Device A. (a) Differential resistance (dV/dI) as a function of bias current I and the microwave power P at $V_{bg} = 0.5$ V when the microwave frequency $f = 3$ GHz, and the corresponding histogram of the voltage (b), here the bin size is 0.14. The two lowest odd Shapiro steps ($n = 1$ and 3) are observed to be suppressed: The first odd step ($n = 1$) is missing nearly over all the microwave power ranges, while the third step ($n = 3$) is slightly weaker than the fourth (with a higher set-in power) instead of being stronger.

IV. RESIDUAL SUPERCURRENT AT THE FIRST NODE

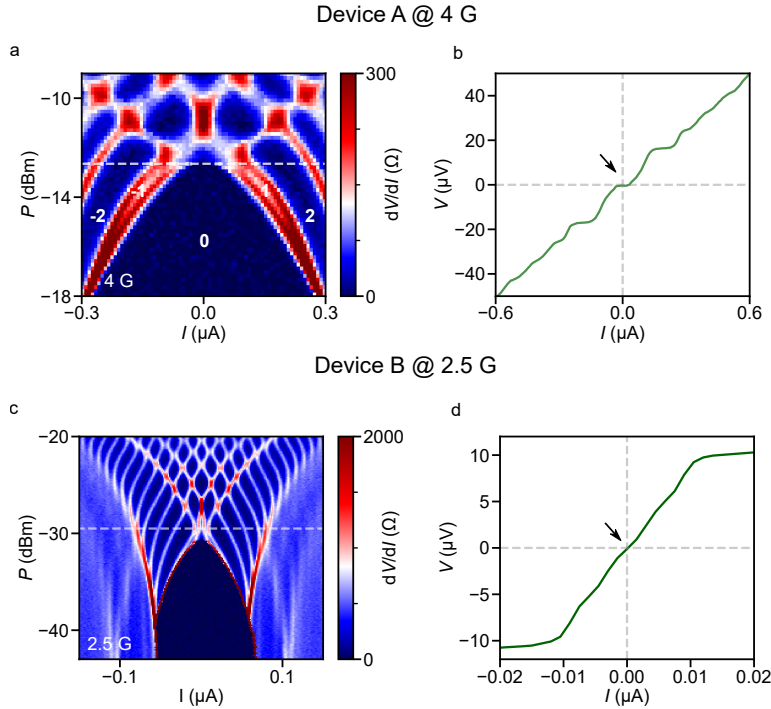


FIG. S3. Residual supercurrent at the first node on Device A at 4 GHz (a,b) and on Device B at 2.5 GHz (c,d). (a) The zoomed-in image of the dV/dI map in Fig. 4b. and (b) the corresponding linecut at the power of -12.65 dBm. (c) Differential resistance (dV/dI) as a function of bias current I and the microwave power P , and the V - I linecut at -29.5 dBm is shown in (d). The residual supercurrent at the first node can be observed as a knot or platform of the V - I curve at zero bias current.

V. SHAPIRO STEPS AT DIFFERENT FREQUENCIES ON DEVICE B

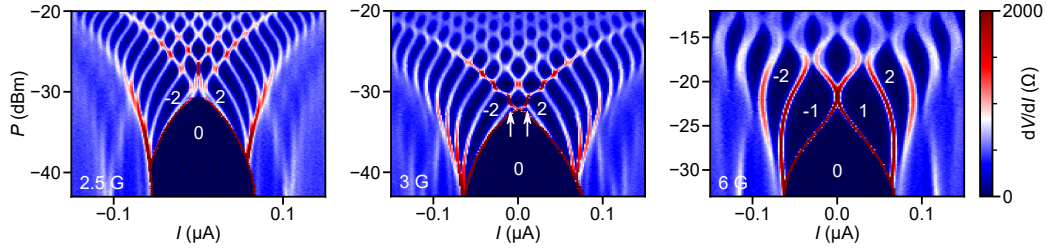


FIG. S4. Differential resistance (dV/dI) as a function of microwave power P and bias current I at the frequencies of 2.5 GHz, 3 GHz, and 6 GHz.

VI. EVOLUTION OF SHAPIRO STEPS IN MAGNETIC FIELDS ON DEVICE B

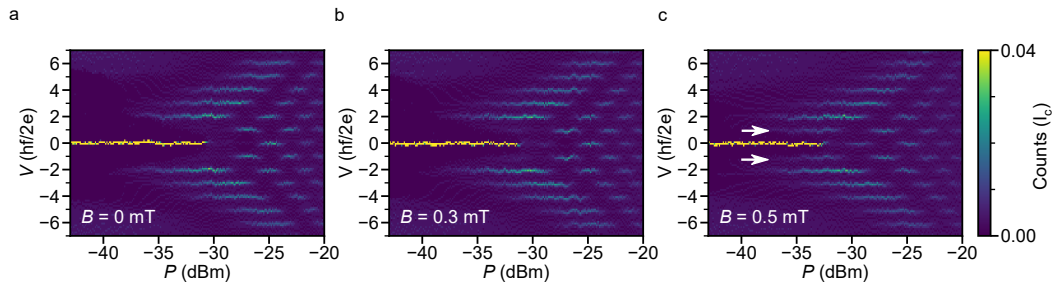


FIG. S5. Normalized voltage histograms at $B = 0, 0.3, 0.5$ mT, under microwave irradiation of the frequency of 2.5 GHz. The first missing Shapiro step reappears as the magnetic field increases. Here, the bin size is 0.14.

VII. DATA FROM DEVICE S1

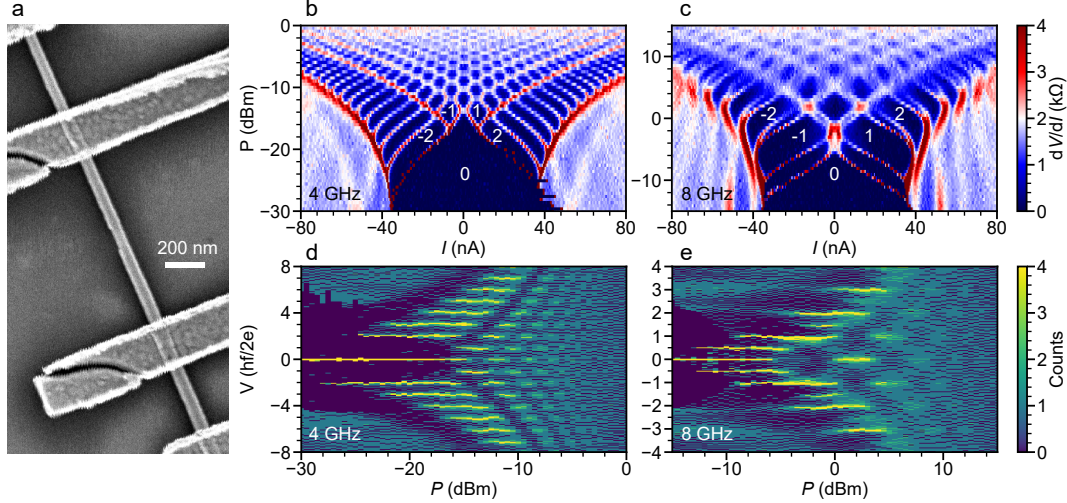


FIG. S6. We also observed the missing first Shapiro step in an epitaxial Al-InAs nanowire device (device S1). (a) SEM image of the device. The InAs nanowire is covered by a layer of epitaxially grown Al (about 15 nm). The narrower section in the middle of the wire is the junction patterned by selective etching. Leads (perpendicular to the wire) are made from Ti/Au. (b) and (c) dV/dI as a function of P and I at 4 GHz and 8 GHz, respectively. (d) and (e) Corresponding histograms of (b) and (c).

VIII. SIMULATION RESULTS

Equations for the resistively and capacitively shunted junction (RCSJ) model, considering a Josephson junction with a sinusoidal current phase relation, can be expressed as follows [53]:

$$\sin \varphi + \frac{d\varphi}{d\tau} + \beta \frac{d^2\varphi}{d^2\tau} = i_{dc} + i_{ac} \sin(\Omega\tau), \quad (\text{S1})$$

$$v = \frac{d\varphi}{\Omega d\tau}, \quad (\text{S2})$$

where φ is the phase difference across the junction, τ is the time, β is the McCumber parameter proportional to the shunted capacitance, i_{dc} and i_{ac} are amplitudes of applied DC and AC currents, respectively, Ω is the angular frequency, v is the normalized voltage equivalent to the Shapiro index. All parameters are dimensionless. This model simplifies to the RSJ model when $\beta = 0$.

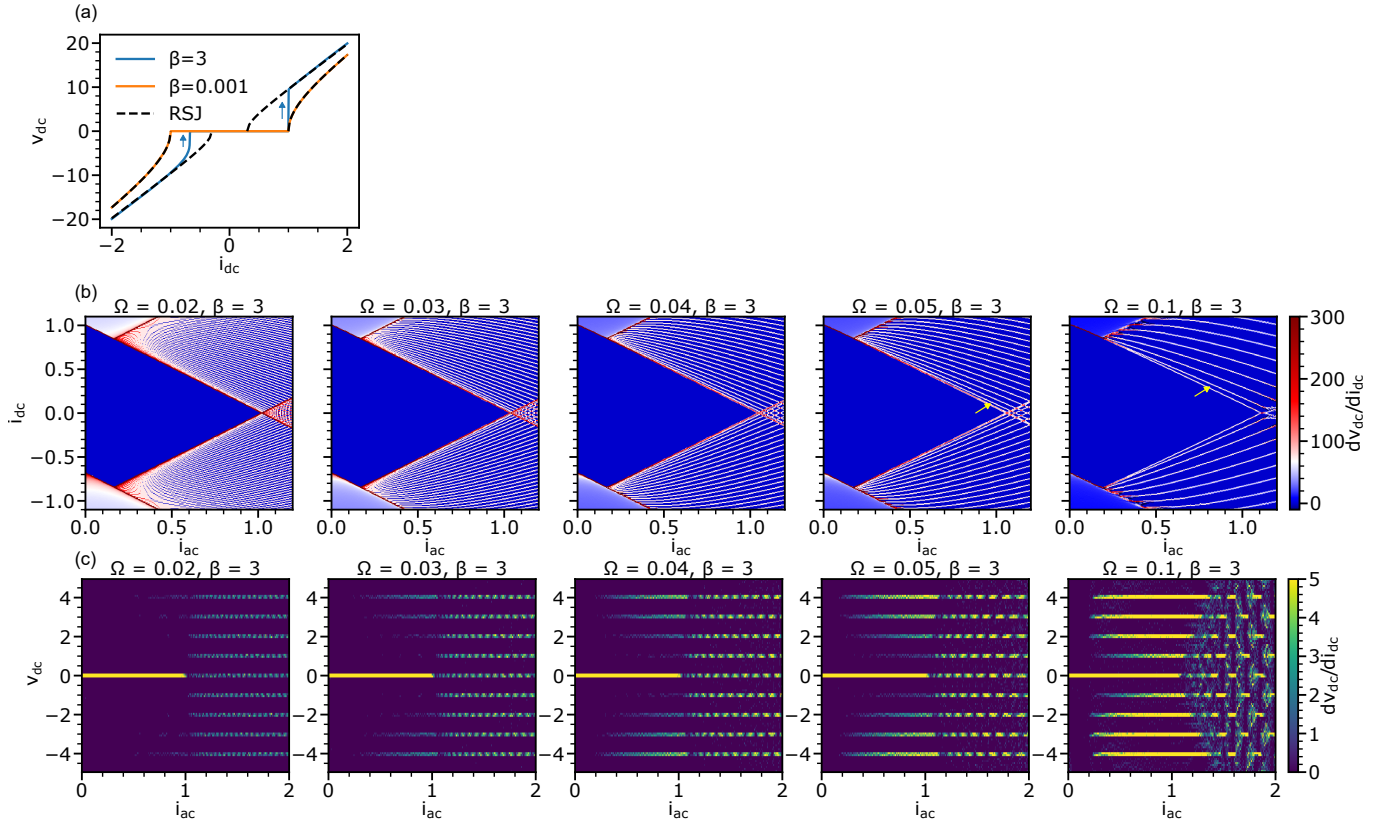


FIG. S7. Simulations showing the impact of the sharp superconducting switching on the first Shapiro step. Here, the jump is introduced by setting a finite β in the RCSJ model. The jump can also be caused by other factors such as the Joule heating. (a) Simulated voltage-current characteristic at $\beta = 3$ and 0.001. Dashed lines are fits using the RSJ relation $v \propto \sqrt{i_{dc}^2 - i_0^2}$. Sharp voltage jumps (blue arrows) near the superconducting switchings occur when $\beta = 3$. (b) Simulated dv_{dc}/di_{dc} maps at a variety of dimensionless frequencies (Ω s) which are noted at the top of each panel. Yellow arrows indicate the positions of the first Shapiro step at $\Omega = 0.05$ and 0.1, which are visible but suppressed compared to the width of the second step. (c) Corresponding histograms of (b). The bin size is 0.1. Lower-order Shapiro steps disappear when the Ω decreases. At $\Omega = 0.03$, the first Shapiro step is missing. At $\Omega = 0.02$, both the first and the second Shapiro steps are missing. The missing Shapiro step regime extends to higher voltages as i_{ac} decreases, which is most evident at $\Omega = 0.03$ and 0.04.

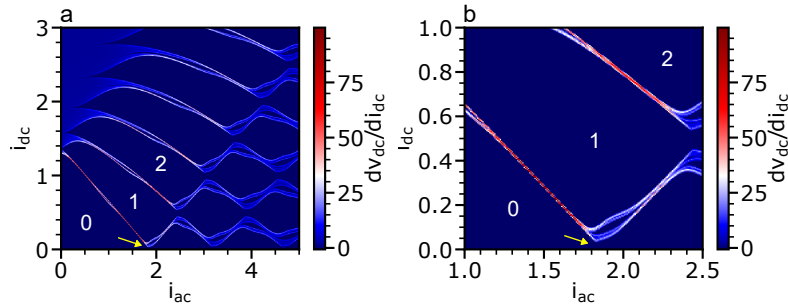


FIG. S8. Residual supercurrent in the RSJ simulation without a 4π Josephson term. (a) Simulated dv_{dc}/di_{dc} as a function of i_{dc} and i_{ac} . Shapiro step indexes are indicated in white. The yellow arrow indicates the first node of the zeroth Shapiro step lobe. (b) Zoomed-in figure of (a). The node is lifted from $i_{dc} = 0$ (yellow arrow), indicating a residual supercurrent at this node. Parameters used for simulation: the CPR is $\sin \varphi + 0.5 \sin 2\varphi$, $\Omega = 0.5$.